Modeling the diurnal variation of tracer transit velocity through a subglacial channel

T. V. Schuler[1,2] and U. H. Fischer[1,3]

Received 19 December 2008; revised 29 May 2009; accepted 19 August 2009; published 21 November 2009.

[1] Tracer injections into a moulin connecting to a subglacial channel at Unteraargletscher were repeated at intervals of about two hours over two diurnal discharge cycles in August and September 2000. The pronounced hysteresis in the relationships between tracer transit velocity and proglacial discharge may be explained by adjustments of the channel cross section in response to discharge variations or alternatively by modulation of inflow from the tributary moulin into a main subglacial channel. To test these hypotheses, we employ a physically based, time-dependent model of channelized subglacial drainage. In a series of numerical experiments, we explore the general characteristics of each mechanism before the model is applied to diurnal discharge variations measured during the tracer tests at Unteraargletscher. We found that the ability of a Röthlisberger channel to adjust its size to the prevailing hydraulic conditions can contribute to the hysteresis in the velocity-discharge relationships. However, using plausible parameter values, R channel hydraulics alone is not satisfactory in reproducing the magnitude of observed transit velocities. The model further confirms that retardation of the tracer in the tributary moulin due to inflow modulation has major effects on transit velocities both in magnitude and timing. With appropriate assumptions on channel sinuosity and moulin size, a combination of both mechanisms can be found that is capable of reproducing the observed transit velocities.

Citation: Schuler, T. V., and U. H. Fischer (2009), Modeling the diurnal variation of tracer transit velocity through a subglacial channel, *J. Geophys. Res.*, *114*, F04017, doi:10.1029/2008JF001238.

1. Introduction

[2] Among the different drainage configurations beneath glaciers, such as water films [*Weertman*, 1972], permeable sediments [*Boulton*, 1974; *Clarke*, 1987], networks of linked cavities [*Walder*, 1986] and different types of channels [*Röthlisberger*, 1972; *Nye*, 1973; *Hooke et al.*, 1990; *Walder and Fowler*, 1994; *Ng*, 2000], those that are channelized are hydraulically most efficient and, hence, dominate in transferring surface meltwaters along the beds of most alpine glaciers. The cross-sectional geometry of subglacial channels evolves in response to variations in glacial discharge; energy dissipated with the water flow enlarges the size of ice-walled channels by melting, while creep of the viscous ice opposes this effect [*Röthlisberger*, 1972; *Spring and Hutter*, 1982]. The resulting changes in channel size and geometry not only affect the transit time of water through the glacier but also the water pressure at the glacier bed. This evolution therefore has important implications for glacier dynamics [e.g., *Iken et al.*, 1983; *Iken and Bindschadler*, 1986; *Iverson et al.*, 1995; *Kavanaugh and Clarke*, 2001; *Mair et al.*, 2002], bulk runoff formation [e.g., *Collins*, 1982; *Arnold et al.*, 1998] and water chemistry [e.g., *Tranter et al.*, 1993].

[3] Hydrologically driven glacier acceleration has recently received considerable attention with the detection of seasonal changes in the velocity field of the Greenland ice sheet [e.g., *Zwally et al.*, 2002; *Joughin et al.*, 2008]. The observed speedup has been related to enhanced meltwater production at the glacier surface in response to climate change and has the potential to increase the contribution of glaciers to sea level rise. However, the relation between glacier hydrology and dynamics does not simply depend on meltwater volume, but is governed by the temporal evolution of the subglacial drainage capacity [e.g., *Truffer et al.*, 2005; *van de Wal et al.*, 2008].

[4] Tracer methods provide a powerful means to investigate the hydraulic characteristics and the temporal evolution of the subglacial drainage system [e.g., *Seaberg et al.*, 1988; *Fountain*, 1993; *Hock and Hooke*, 1993; *Kohler*, 1995; *Nienow et al.*, 1996, 1998; *Schuler et al.*, 2004]. Analyses of transit velocities v and hydrodynamic dispersion obtained from tracer return curves have revealed the existence of different glacial drainage system morphologies [e.g., *Lang et al.*, 1979; *Fountain*, 1993; *Hock et al.*, 1999] and their seasonal changes [e.g., *Hock and Hooke*, 1993; *Nienow et al.*, 1998]. In addition, the relationship between v and discharge Q has been used to characterize the hydraulic conditions in subglacial channels and the extent to which a channel is pressurized [e.g., *Seaberg et al.*, 1988; *Willis et al.*, 1990; *Fountain*, 1993; *Hock and Hooke*, 1993; *Kohler*, 1995]. The method is based

[1]Laboratory of Hydraulics, Hydrology, and Glaciology, Swiss Federal Institute of Technology, Zurich, Switzerland.
[2]Department of Geosciences, University of Oslo, Oslo, Norway.
[3]National Cooperative for the Disposal of Radioactive Waste, Wettingen, Switzerland.

0148-0227/09/2008JF001238

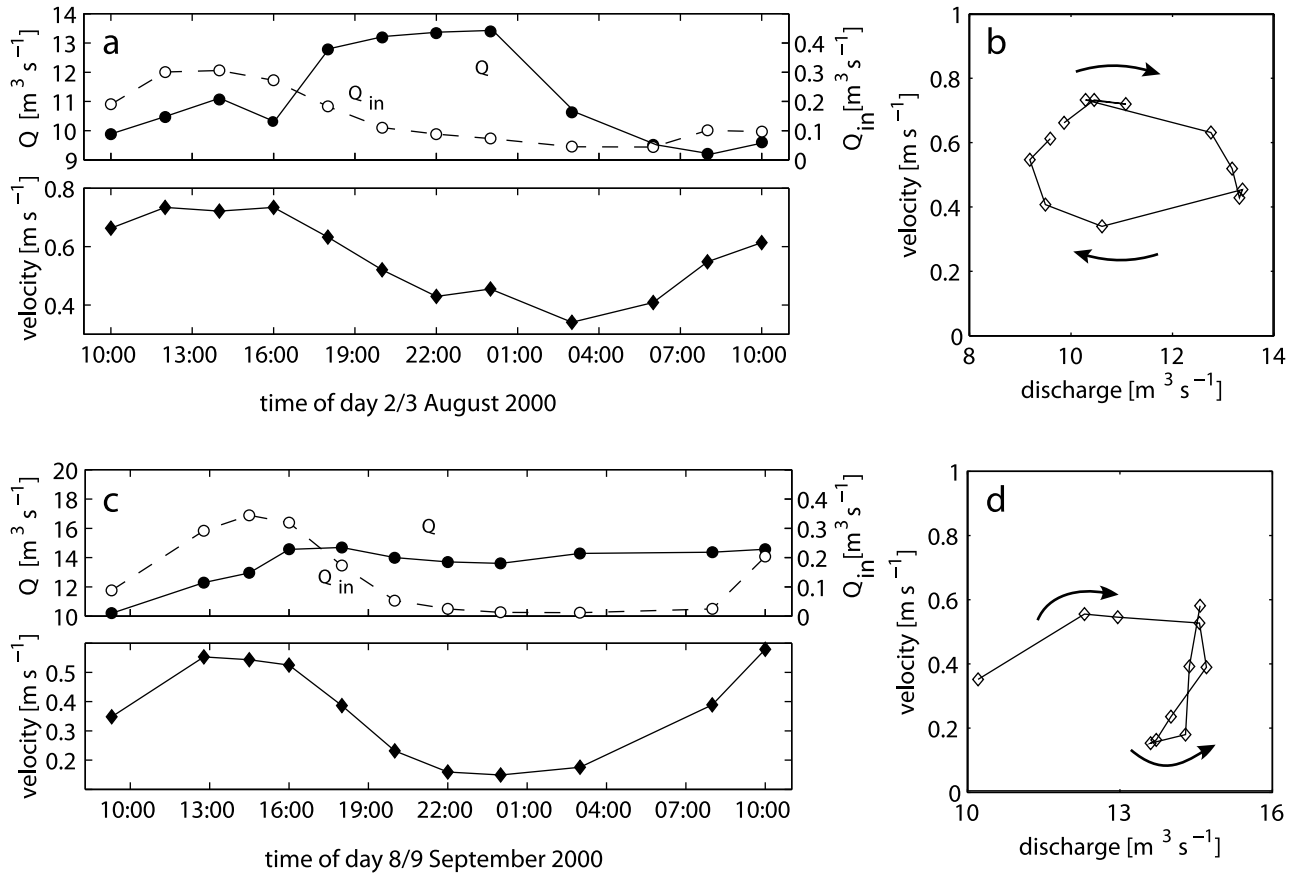

Figure 1. Results of series of tracer tests conducted at Unteraargletscher on (a and b) 2–3 August (*Exp_1*) and (c and d) 8–9 September 2000 (*Exp_2*). Figures 1a and 1c show discharge into the moulin Q_{in} (dashed line), bulk discharge in the proglacial stream Q (solid line), and tracer transit velocity. Figures 1b and 1d show relationships between velocity and bulk discharge. The arrows indicate the chronological order of the data.

on the idea that in a pressurized drainage system, changes in Q proportionally affect v while in an open channel system, variations in Q are partly accommodated by changes in the cross-sectional area occupied by the water. The implication is that changes in the cross-sectional area of the drainage system itself affect the v-Q relationship [*Burkimsher*, 1983]. Hence, the long-term evolution of the drainage system can be tracked by repeating tracer tests over the ablation season [*Nienow et al.*, 1998], whereas the drainage conditions in an evolving channel system at a specific moment can be inferred from a snapshot of the corresponding v-Q relationship [*Kohler*, 1995]. However, even if the data are collected within a short period, v-Q relationships are found to display a wide scatter thereby complicating the interpretation of hydraulic conditions [*Collins*, 1982; *Nienow et al.*, 1996; *Schuler et al.*, 2004]. *Nienow et al.* [1996] and *Schuler et al.* [2004] suggested that modulation of inflow from a tributary to a main channel [*Smart*, 1990] could induce such scatter. Additionally, *Schuler et al.* [2004] proposed that changes in the channel cross-section affect the transit velocity and may be responsible for the observed complexity.

[5] In this paper, we implement channel evolution and inflow modulation in a numerical model and analyze each of the proposed mechanisms individually and examine their respective abilities to account for the observed v-Q relationships associated with experiments on Unteraargletscher, Switzerland [*Schuler et al.*, 2004].

2. Background

[6] Unteraargletscher, Switzerland, extends about 6 km eastwards from the confluence of Lauteraargletscher and Finsteraargletscher. It has a mean width of 1 km and a surface slope of approximately 4°. Close to the confluence area, the ice is more than 400 m thick and thins gradually towards the glacier snout with a thickness of ~200 m 1.5 km from the terminus [*Bauder et al.*, 2003].

[7] To obtain insight into the hydraulics of the subglacial drainage system beneath Unteraargletscher, we conducted tracer tests from a large moulin that was located at the glacier centerline, 4450 m upglacier from the terminus [*Schuler et al.*, 2004]. On 2–3 August and 8–9 September 2000, we performed two series of tracer injections at intervals of ~2 h, each over an entire diurnal discharge cycle to obtain a snapshot of the v-Q relationship (Figure 1). The tracer injections were accompanied by measurements of proglacial discharge Q and supraglacial discharge Q_{in} using the salt dilution method. Details of the field methods are described by *Schuler et al.* [2004]. These two series of tests are subsequently referred to as *Exp_1* and *Exp_2*, respectively. The generally

high transit velocities (Figures 1a and 1c) in conjunction with a low tracer dispersion [*Schuler and Fischer*, 2002] suggest flow through an hydraulically efficient, channelized drainage system. However, a simple functional relationship between v and Q cannot be determined due to the wide scatter of the data points in plots of v versus Q for both experiments (Figures 1b and 1d). Nevertheless, this scatter is not stochastic and if the chronological order of the tracer injection is taken into account, the data reveal a systematic pattern exhibiting hysteretic behavior. The circular v-Q hysteresis in a clockwise direction of *Exp_1* (Figure 1b) illustrates a phase shift of about 0.5 π between the velocity and discharge signals. The nonlinear v-Q relationship of *Exp_2* (Figure 1d) is caused by a marked decrease and subsequent rise of v during a phase when Q remained at an almost constant level.

[8] In an earlier paper [*Schuler et al.*, 2004], we interpreted v-Q hysteresis in terms of two possible mechanisms acting separately or in combination. First, since the slope of the v-Q relation directly reflects the hydraulic geometry of a given drainage system, diurnal variations in the channel cross-sectional area would produce a hysteretic v-Q relationship. Second, we observed that velocity variations were more closely in phase with supraglacial discharge Q_{in} than with proglacial discharge Q (Figures 1a and 1c). This observation may be explained if inflow from the tributary moulin into the main channel was modulated in such a way that the tracer transit time through the tributary is a large enough fraction of the overall transit time [*Smart*, 1990; *Fountain*, 1993; *Nienow et al.*, 1996; *Schuler et al.*, 2004].

[9] To date, the precise mechanisms that account for observed v-Q hysteresis remain largely unexplored. *Nienow et al.* [1996] modeled tracer transport through a two-component channel system where distinct v-Q relationships for each component were prescribed, and were able to reproduce observed hystereses. In this paper, we use a physically based model of channelized subglacial drainage to compute tracer transit velocities in response to prescribed variations in discharge. In doing so, we first analyze separately the effects of an adjustable channel cross section and the consequences of inflow modulation on tracer transit velocity. Subsequently, we consider a combined moulin channel system to investigate the drainage conditions that produce the observed v-Q behavior.

3. Modeling Drainage Through a Subglacial Channel

[10] Drainage through a subglacial channel is simulated using a physically based model that describes the flow of water through a channel of adjustable cross section. The model is forced by prescribed discharge time series and consists of two coupled equations that describe the evolution of the channel cross section and the pressure distribution along the channel. From the resulting channel geometry and pressure distribution, we calculate tracer transit velocities, and compare them to those measured in the field.

[11] Water drainage through an ice-walled channel is described as flow of a fluid through its solid phase [*Spring and Hutter*, 1982]. The first comprehensive theory was presented by *Röthlisberger* [1972], who considered an equilibrium state between melt enlargement and creep closure. The resulting inverse relationship between water pressure and discharge has important implications for glacial hydrology and channels of this type have subsequently been named Röthlisberger channels or R channels. However, glacial meltwater production varies on time scales much shorter than the time needed for such a channel to reach steady state conditions [*Spring*, 1980]. To consider diurnal variations of discharge, we employ a time-dependent model.

3.1. Assumptions

[12] A channelized subglacial drainage route is most commonly envisaged as an irregular meandering channel of complex cross-sectional shape and size, located at the glacier bed and incised into the overlying ice. It has been suggested that the cross-sectional shape of subglacial channels may be wide and low [*Hooke et al.*, 1990; *Cutler*, 1998] rather than semicircular or circular [*Röthlisberger*, 1972]. The closure rate of a wide, low channel is faster than that of a semicircular one of equivalent cross-sectional area [e.g., *Hooke et al.*, 1990]. In addition, such a geometry is more resistive to water flow.

[13] The lack of detailed information on the real course and geometry of a subglacial channel requires that we make the simplest possible assumptions. Also for simplicity, we adopt a semicircular geometry for the cross section of the channel and investigate afterwards the effects of a different cross-sectional geometry on our results. In detail, the following assumptions are included in our model formulation:

[14] 1. Melt water entering the channel is close to the melting point and any frictional heat produced is consumed locally, thus advection of thermal energy is neglected.

[15] 2. The ice is isothermal and at the pressure melting point. This is typical for most glaciers in the Alps. Hence, the energy dissipated by the flow of water is entirely available for melting channel walls.

[16] 3. Velocity and pressure are distributed uniformly across the channel cross section; hence, the problem can be reduced to one dimension in the flow direction.

[17] 4. The contribution to discharge from melting of channel walls is negligible.

[18] 5. The channel is directed parallel to ice flow and far-field longitudinal and transverse strain rates are negligible, thus the channel axis is stationary.

[19] 6. The channel has a semicircular cross section, i.e. for the computation of channel closure rates, we use *Nye*'s [1953] analytical expression for the closure of a cylinder.

[20] 7. The channel axis is straight and effects of curvature, bends and breaks on water flow are not described explicitly.

[21] 8. Any kind of hydraulic head loss is described by a single friction parameter using the Darcy-Weisbach formulation. In doing so, we incorporate all loss terms such as those due to channel curvature or other longitudinal and cross-sectional irregularities.

[22] 9. The kinetic potential of the flowing water is small compared to the potentials of pressure and topography and can be neglected.

[23] 10. Negative water pressure or suction cannot occur. Instead, water flows under open channel conditions and fills the channel partially. In this case, melting occurs only at the wetted part of the channel perimeter.

[24] 11. The channel cross section is assumed to remain semicircular, regardless of whether open channel flow occurs or not.

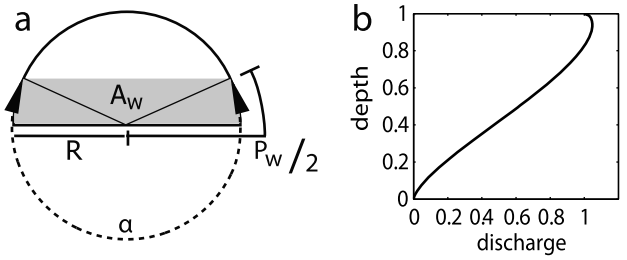

Figure 2. Water flow through a partially filled semicircular channel. (a) Cross-sectional view. The shaded area represents A_w, the area occupied by the water. (b) Discharge as a function of filling depth. The values are scaled with respect to those that correspond to complete filling.

3.2. Model Equations

3.2.1. Channel Geometry

[25] Following *Röthlisberger* [1972] and *Nye* [1976] the evolution of the cross-sectional area A of a semicircular R channel can be expressed as

$$\frac{\partial A}{\partial t} = C\,\frac{\rho_w g}{\rho_i L_f} Q(t)\left((1 - c_t c_w \rho_w)\frac{\partial h}{\partial x} + \frac{\partial z}{\partial x}\right) - 2AB\left(\frac{\rho_w g}{n}(h^* - h)\right)^n. \quad (1)$$

The first term on the right hand side accounts for the melt enlargement of the channel due to dissipation of potential energy, where the water pressure p_w is written in terms of hydraulic head $h = p_w/(\rho_w g)$ with ρ_w denoting the density of water and g the acceleration due to gravity. Further, ρ_i is the density of ice, L_f is the latent heat of melting, c_t expresses the change in melting temperature per unit pressure, c_w is the specific heat of water and x and z denote the coordinate measured upglacier from the snout and the elevation of the bed, respectively. The correction factor $C = P_w/P$ represents the ratio of wetted perimeter P_w to total perimeter P and accounts for reduced melting during open channel flow conditions. The ice overburden pressure expressed in terms of hydraulic head $h^* = (\rho_i/\rho_w)h_i$ is exerted by ice of the thickness h_i, and B and n are the parameters in Glen's flow law.

3.2.2. Water Flow

[26] To relate hydraulic potential to discharge, we use the Darcy-Weisbach formula [e.g., *Chow et al.*, 1988]

$$\frac{\partial H}{\partial x} = \frac{f}{8g}\frac{Q^2 P_w}{A_w^3}, \quad (2)$$

where the total potential $H = h + z$, $A_w = Q/v$ denotes the cross-sectional area occupied by the water and f is a dimensionless friction factor. This relation is valid for fully turbulent water flow. Given a critical Reynolds number of about 2000 for the transition from laminar to turbulent flow [e.g., *Chow et al.*, 1988], it turns out that even in a small channel of 0.1 m in diameter a velocity higher than 0.04 m s^{-1} would cause turbulence. Water flow velocities observed in glaciers are typically higher [e.g., *Hock and Hooke*, 1993; *Fountain*, 1993; *Nienow et al.*, 1996; *Schuler et al.*, 2004]. Hence, flow in subglacial channels carrying significant water quantities will be turbulent [*Weertman*, 1972].

[27] Flow conditions through a channel are pressurized, where discharge exceeds the maximum amount Q_{max} that can be routed under open channel flow conditions. For a given channel cross section, we derive this threshold from equation (2) by considering $h = 0$ and recalling that for a completely filled, semicircular channel $A_w = A$ and $P_w = P = (\pi + 2)R$ with radius $R = (\frac{2A}{\pi})^{1/2}$:

$$Q_{max} = (2A)^{5/4}\frac{\pi^{1/4}}{(\pi+2)^{1/2}}\left(\frac{g}{f}\left|\frac{\partial z}{\partial x}\right|\right)^{1/2}\mathrm{sgn}\left(\frac{\partial z}{\partial x}\right). \quad (3)$$

When $Q > Q_{max}$, pressurized flow takes place. In this case, equation (2) becomes

$$\frac{\partial H}{\partial x} = \frac{f}{g}(2A)^{-5/2}\frac{\pi+2}{\pi^{1/2}}Q^2, \quad (4)$$

and $C = 1$ in equation (1).

[28] In the case of open channel flow ($Q \le Q_{max}$), the computation of C requires P_w, the wetted perimeter of the partially filled channel cross section. The cross-sectional area occupied by water A_w in a partially filled semicircular channel, is given by

$$A_w = A\left(\frac{\alpha - \sin\alpha}{\pi} - 1\right), \quad (5)$$

where the angle α is defined as shown in Figure 2a. From equation (2) with $\partial H/\partial x = \partial z/\partial x$ and equation (5) we obtain

$$\frac{\partial z}{\partial x}\frac{8g}{f}Q^{-2} = P_w\left(A\left(\frac{\alpha - \sin\alpha}{\pi} - 1\right)\right)^{-3}, \quad (6)$$

where $\alpha = P_w/R + \pi - 2$. P_w is then obtained by iteration using the bisection method. Figure 2b illustrates that the relation between discharge and filling depth in a partially filled semicircular channel is not unique for high filling levels. At such high filling levels, P_w increases faster with filling depth than A_w. In consequence, when water fills the channel to a depth of ~94%, $P_w \sim 0.82\,P$ and a slightly larger discharge is drained than that at higher filling levels (Figure 2b). This point marks the transition to pressurized flow when the filling depth in a partially filled channel increases. In contrast, the transition from pressurized to open channel flow takes place at a discharge which corresponds to complete filling [*Chow*, 1988]. We recall that we describe this transition using one single value Q_{max} (equation (3)) instead of two different ones for opening and closing. The resulting error in the calculated hydraulic head is of the order of 10^{-5} m for typical values of A (5–10 m^2). We neglect this inaccuracy because it is small compared to typical variations of hydraulic head which are of the order of several meters.

3.2.3. Tracer Transit Through a Channel

[29] Once the channel geometry and pressure profile are determined, the local flow velocity of the water can easily be calculated as

$$v_{loc} = \frac{Q}{A_w}. \quad (7)$$

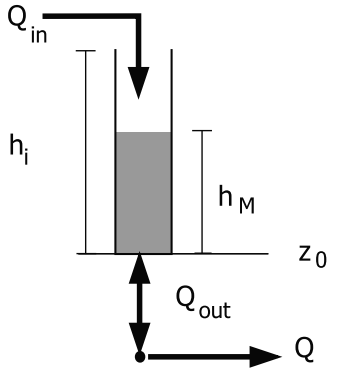

Figure 3. Sketch of the moulin model configuration.

Where the water flow through the channel is pressurized, water occupies the entire cross section and $A_w = A$. Where open channel flow occurs, A_w follows from equation (5) and $\alpha = P_w/R + \pi - 2$. Finally, the transit velocity v at which a tracer travels through the channel is simply calculated as the spatial mean of v_{loc} along the channel. As we will see later, the modeled residence time rarely exceeds the duration of one output time increment. Hence, a Lagrangian description to calculate the transit velocity is not necessary.

3.2.4. Tracer Transit Through a Moulin

[30] Often in tracer experiments, dye is injected into a supraglacial stream as it enters a moulin. A moulin that joins a major channel might act as a piezometer; its water level thereby reflects the water pressure in the channel. The transit velocity of a tracer through this water column in the moulin is controlled by supraglacial input discharge. The residence time of the tracer is thus the result of variations in both subglacial water pressure and supraglacial discharge, and we refer to this effect as inflow modulation. *Nienow et al.* [1996] and *Schuler et al.* [2004] proposed that inflow modulation at the junction of a tributary to the main channel might explain the observed *v*-*Q* hysteresis.

[31] To model the transit velocity of a tracer, we describe the system as a moulin and a subglacial channel that are connected at a given distance from the terminus (Figure 3). Where the moulin joins the pressurized channel, water backs up in the moulin to a certain hydraulic head h_M. This hydraulic head drives the total discharge Q through the channel downstream from the moulin and is related to Q and the channel geometry A through equation (4).

[32] The rate of water exchange between the moulin and the subglacial channel Q_{out} is governed both by the surface input into the moulin Q_{in} as well as by the evolution of h_M and is derived from the water balance of the moulin:

$$Q_{out} = \begin{cases} 0 & : \quad h_M \geq h_i \\ Q_{in} & : \quad h_M \leq 0 \\ Q_{in} - \frac{dh_M}{dt} A_M(h_M) & : \quad \text{otherwise,} \end{cases} \tag{8}$$

where A_M is the cross-sectional area of the moulin. The water column in the moulin cannot exceed the local ice thickness h_i.

[33] To determine the residence time of a tracer in the moulin, we employ a Lagrangian description and follow the tracer on its way down the water column. We do this by labeling the water level h_M at the time of "tracer injection" as the elevation of the tracer above the bottom, $z_T = z_0 + h_M$. We then calculate the rate at which the tracer is lowered

$$\frac{dz_T}{dt} = \frac{Q_{out}(t)}{A_M(h_M)} \tag{9}$$

and compute the time needed for the tracer to reach the bottom of the moulin ($z_T = z_0$).

3.3. Numerical Implementation

[34] For prescribed distributions of ice thickness $h_i(x)$, glacier bed elevation $z(x)$ and a time varying discharge $Q(t)$, we can solve the model equations for the unknowns $A(x)$, $h(x)$ and $v_{loc}(x)$ which denote the distributions along the channel of cross-sectional area, hydraulic head and flow velocity, respectively. While $v_{loc}(x)$ is readily computed from equation (7), $A(x)$ and $h(x)$ are obtained from the coupled equations (1) and (4) where the water flow is pressurized and from equation (1) and $h = 0$ otherwise. Equation (3) is used to discriminate between these two cases. Where open channel flow occurs, the value of P_w is calculated from equation (6). Given initial conditions for $A(x)$ and $h(x)$ and a boundary condition at the lower end of the channel (e.g., $h_{x=0} = 0$ in accordance with the observation that the water is exiting Unteraargletscher at atmospheric pressure), the coupled equations for $A(x)$ and $h(x)$ are solved following the numerical method of lines [e.g., *Schiesser*, 1991]. The equations are spatially discretized along the channel using finite difference approximations thereby converting the system of partial differential equations into a mixed system of differential algebraic equations.

[35] Special caution is required for the choice of consistent initial conditions, otherwise the numerical integration is likely to fail promptly [*Clarke*, 1996]. Using rough estimates of initial values of $h(x)$ and $A(x)$, we start the numerical integration with a given constant discharge Q and let the system approach steady state. Transient computations are then started from this steady state.

[36] When modeling the retardation in a tributary moulin, we have to prescribe Q_{in} and A_M, together with the initial distributions of $A(x)$ and $h(x)$ along the channel and total discharge Q. The water level in the moulin h_M is identical to the hydraulic head at the junction of moulin and channel.

[37] The physical constants used in all model runs are listed in Table 1. For the computations, we use a spatial resolution of $\Delta x = 50$ m, a value that ensures sufficiently accurate solutions as indicated by preliminary experiments. The system of differential algebraic equations was solved using *ode15s* in MATLAB; the solver selects the time steps internally. We assume further that the friction factor f as well as the material properties of ice, expressed as n and B, are constant along the channel. The values for the flow law

Table 1. Physical Constants

Physical Property	Value	Unit
Gravitational acceleration g	9.8	m s^{-2}
Density of ice ρ_i	900	kg m^{-3}
Density of water ρ_w	1000	kg m^{-3}
Latent heat of melting L_f	333.5	kJ kg^{-1}
Pressure melting coefficient c_t	-7.4×10^{-8}	K J^{-1} m^3
Specific heat of water c_w	4.22×10^3	J kg^{-1} K^{-1}

Table 2. Model Parameters

Parameter	Value	Unit
Friction factor f	0.5	-
Flow law exponent n	3	-
Flow law coefficient B	5.3×10^{-24}	$Pa^{-3}\ s^{-1}$

parameters are adopted from *Nye* [1953] and the choice for f follows from *Spring and Hutter* [1982] (Table 2).

4. Application to Unteraargletscher

[38] In this section, we use the model described above to investigate separately the effects of an adjustable channel geometry and of inflow modulation on tracer transit velocity. The model is applied to a geometry representing Unteraargletscher and we use observed time series of discharge to simulate *Exp_1* and *Exp_2*. We characterize the results in terms of absolute values of v, its range and the phase relation between v and Q and compare these to the observations. First, we test the effect of an adjustable channel geometry assuming plausible values for the parameters f, B, and channel sinuosity S. In a sensitivity study, we explore the realms of possibility by applying extreme values that still are considered physically feasible. Second, we study the effect of inflow modulation at the junction of a moulin to a main channel by varying the cross-sectional area A_M of the moulin which in turn is fed by the supraglacial discharge Q_{in}. In a third step, we combine the two mechanisms by modeling a moulin connected to an R channel to simulate the evolution of transit velocity as observed during *Exp_1* and *Exp_2*.

[39] The straight-line distance from the moulin into which the tracer was injected to the glacier terminus is approximately 4.5 km. It is assumed that the water flows through a subglacial channel which follows the thalweg along the glacier bed. Since the glacier bed beneath the tongue of Unteraargletscher is steadily inclined [*Bauder et al.*, 2003], a constant value of $\partial z/\partial x = 0.012$ was used. The distribution of h^* along the centerline of Unteraargletscher is represented by a parabolic function that was fitted to ice thickness data. Initial distributions of $A(x)$ and $h(x)$ are taken from the steady state calculated for $Q = 12\ m^3\ s^{-1}$ for *Exp_1* and $Q = 11\ m^3\ s^{-1}$ for *Exp_2*.

4.1. Channel Geometry Changes

[40] To define a reference situation, we simulate *Exp_1* using parameter values listed in Table 2. We further make the assumption that the sinuosity of the channel $S = 1$, implying that the channel axis follows a straight line between the sites of tracer injection and detection.

[41] For a channel of adjustable geometry, Figure 4a shows the time series of hydraulic head, channel cross-sectional area and transit velocity modeled for the discharge observed during *Exp_1*. Pressure values h/h^* at the upstream end of the channel vary between 21% and 63% of the flotation level at this location. Velocity v ranges from approximately 1.6 m s^{-1} during the discharge minimum to 2.2 m s^{-1} at peak discharge. The cross-sectional area A varies around the steady state size of $\sim$5 m^2 and responds to the discharge cycle with a delay of $\sim$5 h. This time lag also causes a phase shift between Q and h. During rising discharge, the channel cross section is smaller than at the falling limb of Q and thus, a higher hydraulic head is required to drive the same discharge. Therefore, h precedes Q by about 1–2 h thereby also causing a comparable lag between v and Q.

[42] Longitudinal profiles of the glacier geometry and hydraulic head reveal that open channel flow occurs in the lowermost 500 m during peak discharge, while it extends to 1250 m during minimal discharge (Figure 4b). The resulting velocity profiles illustrate the hybrid nature of the flow regime (Figure 4c). In the open channel, v_{loc} is almost constant. A noticeable drop marks the transition to pressurized flow. The transition from open channel to pressurized flow does not occur steadily but rather the water level in a

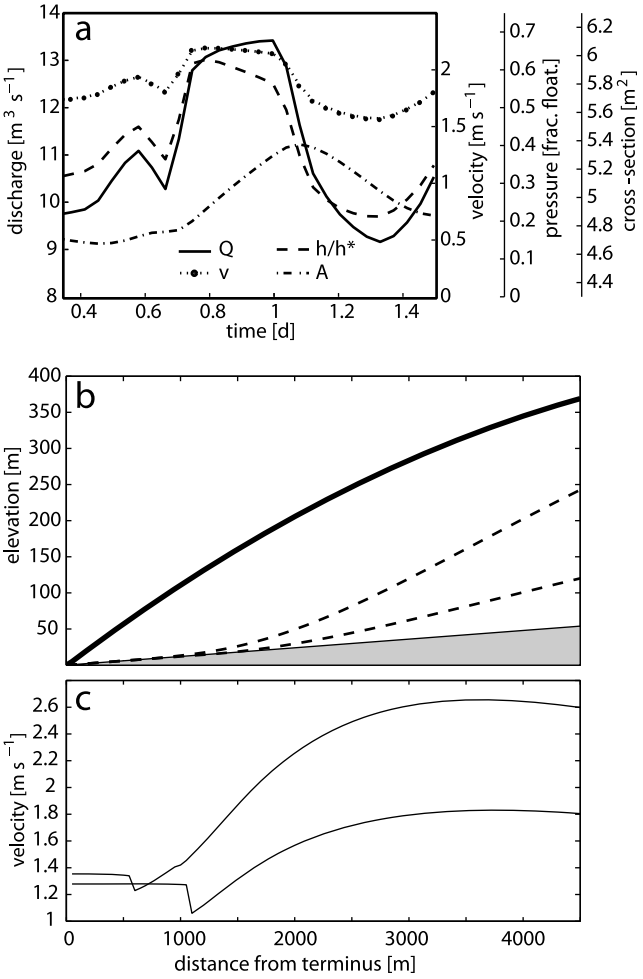

Figure 4. Results of modeling channel geometry changes. (a) Variations in transit velocity v, hydraulic head (expressed as fraction of flotation pressure) h/h^*, and cross-sectional area A in response to the discharge Q measured during *Exp_1*. The displayed values of h/h^* and A are those calculated for a distance of 4.5 km from the terminus. (b) Longitudinal profiles of glacier bed (shaded), glacier surface (solid), and hydraulic potential (dashed). The range of hydraulic potential is illustrated by the profiles at maximum (top profile) and minimum (bottom profile) discharge. (c) Distribution of flow velocity v_{loc} along the R channel. The two situations correspond to maximum (top profile) and minimum (bottom profile) discharge.

Table 3. Sensitivity of *Exp_1* Model Results to Uncertainties in Flow Path Sinuosity S, Channel Roughness f, and Flow Law Coefficient B[a]

Description	Parameter Value	Pressure Range[b]	Velocity Range (m s^{-1})	v-Q Phase Shift (π)
Reference	$S = 1$ $f = 0.5$ $B = 5.3 \times 10^{-24}$	0.21–0.63	1.56–2.17	−0.1
Sinuous path	$S = 2$	0.33–0.91	0.65–0.95	−0.1
	$S = 3$	0.40–1.03	0.39–0.56	−0.1
Enhanced roughness	$f = 1.1$	0.25–0.69	1.18–1.64	−0.1
Reduced roughness	$f = 0.12$	0.14–0.44	2.59–3.46	−0.1
Softer ice	$B = 6.8 \times 10^{-24}$	0.24–0.66	1.61–2.21	−0.1
Stiffer ice	$B = 2.4 \times 10^{-24}$	0.12–0.40	1.43–1.92	−0.1
Hooke-channel	$B = 16 \times B_{ref}$	0.53–1.06	2.04–2.62	−0.2
Observation	-	-	0.34–0.75	−0.5

[a]Flow path sinuosity and channel roughness are dimensionless, flow law coefficient is measured in $Pa^{-3}s^{-1}$.
[b]Pressure is expressed relative to flotation pressure.

partly filled channel cross section switches suddenly to complete filling when the critical discharge Q_{max} (cf. equation (3)) is reached. As such, A_w suddenly increases and considering the same discharge, continuity requires that the velocity drops across the transition. Where the water flow is pressurized, v_{loc} reflects directly $\partial h/\partial x$. Hence, upglacier from the transition, velocities increase steeply in the upglacier direction. Further upglacier, the rise decreases gradually until a maximum is reached at approximately 3.7 km from the glacier terminus. The differences between maximum and minimum velocities at a given location scale with the diurnal amplitude of hydraulic head and range from ~0.1 m s^{-1} at the outlet to ~0.8 m s^{-1} at 4.5 km distance from the terminus.

[43] To explore the effects of parameter uncertainties on simulated hydraulic head, transit velocity and the phase relation between v and Q, we carried out a sensitivity study by varying the parameters used in the reference situation discussed above (Table 3). We account for a possible sinuosity S of the flow path by modeling a channel having a length of S times the straight line length and slope $(1/S)$ $(\partial z/\partial x)$. Since the course of the subglacial channel in nature is unknown, physical constraints on S are not available. We therefore consider two arbitrary situations $S = 2$ and $S = 3$. We find that an increase in sinuosity leads to generally higher pressure levels as well as to an increase in the amplitude of the pressure variation. As expected, increasing channel sinuosity reduces the associated transit velocity, coinciding with a reduction of the diurnal velocity range. At the given temporal resolution of the results (1 h), we are not able to detect an effect on the v-Q phase relationship.

[44] The roughness coefficient f is varied between values representing the high form drag of an irregularly shaped channel and the low skin friction expected for an ice-walled channel. Model results indicate that an enhanced roughness increases the pressure level whereas it has an reducing effect on both the transit velocity and the amplitude of the velocity variation. There is virtually no effect on the v-Q phase shift.

[45] The flow law coefficient B is changed to values representing a slightly softer and a slightly stiffer ice. As a reference, we use a value determined by *Nye* [1953] using measured closure rates of ice-walled tunnels although there exists a value determined for Unteraargletscher by comparing measured and modeled surface velocities [*Gudmundsson*, 1999]. However, in his model formulation, *Gudmundsson* [1999] neglected basal motion and, therefore, had to assume a value of B that likely overestimated ice deformation to achieve agreement between measured and modeled surface velocities. Therefore, we regard this value to represent softer ice. The value for stiffer ice is adopted from *Paterson* [1994]. *Hooke et al.* [1990] demonstrated that the enhanced closure of a broad and low channel geometry can be represented by modifying the value of B in *Nye*'s [1953] expression for channel closure by a factor of 16. We find that changes in B affect pressure and velocity such that an enhanced closure rate leads to higher water pressures and a higher transit velocity. The effects of changes in B on the v-Q phase shift are negligible, except for the extreme closure rate taken to represent a *Hooke et al.* [1990]-type channel. However, the phase shift is still substantially smaller than the observed one and was achieved at the cost of considerably overestimated transit velocities.

4.2. Inflow Modulation

[46] To investigate the influence of a moulin on the transit velocity of a tracer, we performed a number of simulations using different cross-sectional areas of the moulin A_M. Since our aim in this section is to examine the influence of inflow modulation on tracer transit, we consider the channel downstream of the moulin to be a rigid pipe instead of a channel of adjustable geometry and thus neglect the dynamics of the channel cross section (equation (1)). We further assume that the moulin extends to the glacier bed, has constant and uniform cross-sectional area and is located at 4.5 km from the terminus. The model is driven by continuous time series of Q and Q_{in} which were obtained by linearly interpolating between the data points of the measured supraglacial and proglacial discharges, respectively, shown in Figure 1a.

[47] We use simulations of *Exp_1* to demonstrate the effect of inflow modulation on the transit velocity for different values of A_M (Figure 5). As expected, variations of hydraulic head in a rigid pipe follow directly those of discharge and therefore, the water column height in the moulin h_M also varies in phase with Q (Figure 5a). With increasing size of the moulin cross-sectional area A_M, the transit velocity through the entire system changes noticeably in magnitude and phase (Figure 5b). As a primary effect we note that as A_M is increased the mean transit velocity decreases. In addition, the v-Q phase relationship is also affected by A_M such that v varies in phase with Q for $A_M = 0$ whereas an antiphase relationship develops with increasing A_M. We also observe

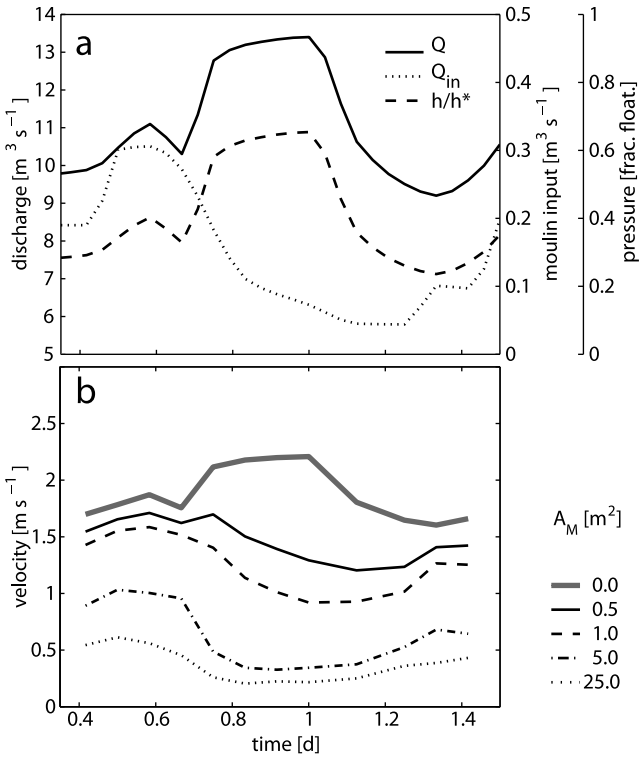

Figure 5. Results of modeling inflow modulation. (a) Variations in hydraulic head (expressed as fraction of flotation pressure) h_M/h^* at the junction of moulin and channel (dashed) in response to the discharge in the channel Q (solid) and input into the moulin Q_{in} (dotted) measured during *Exp_1*. (b) Variations in transit velocity in response to Q and Q_{in} shown in Figure 5a for different values of the moulin cross-sectional area A_M. As a reference, $A_M = 0$ considers the channel without the tributary moulin.

that for a very large moulin ($A_M = 25$ m^2), the amplitude of the velocity variation is attenuated.

4.3. Simulation of *Exp_1* and *Exp_2*

[48] In a further numerical experiment, we combine the two mechanisms, adjustable geometry of an R channel and inflow modulation in the tributary moulin, to simulate *Exp_1* and *Exp_2*. Values for the parameters channel sinuosity S and cross-sectional area of the moulin A_M were adjusted to achieve agreement between modeled and observed transit velocity. As an additional constraint we use the condition $h < h^*$ at the location of the junction of moulin and subglacial channel, in agreement with qualitative observations in the field during the experiments. For the remaining parameters f, n and B, we use the values presented in Table 2. Considering the many assumptions and uncertainties inherent in our model, we conducted only a rough, manual parameter adjustment instead of applying a formal optimization scheme.

[49] Figure 6 presents the results obtained using $S = 1.6$ and $A_M = 4$ m^2 and 5 m^2 for the simulation of *Exp_1* and *Exp_2*, respectively. In *Exp_1*, the cross-sectional area of the channel is larger on the falling than on the rising limb of Q (Figure 6a), thereby causing a slight phase shift between h and Q. Due to the overall rising trend of the discharge in *Exp_2*, A is growing steadily and the corresponding water pressure h varies in similar ways to Q (Figure 6c). In both cases, *Exp_1* and *Exp_2*, the modeled transit velocities generally provide a good match with the observations both in terms of magnitude and timing (Figures 6b and 6d).

5. Discussion

[50] To our knowledge, this paper presents the first attempt to simulate the evolution of tracer transit velocities through a subglacial channel of adjustable cross section. The model describes not only channel adjustment to prevailing hydraulic conditions but also considers the modulation of inflow at the junction of a tributary moulin into the main subglacial channel. This two-component approach has been recently adopted also by M. Werder et al. (manuscript in preparation, 2009) in a lumped element model to interpret tracer experiments at Gornergletscher, Switzerland.

5.1. Channel Geometry Changes

[51] Comparison of model results and measurements indicates that the magnitude of modeled velocities systematically exceed values derived from the tracer experiments. These differences are mainly associated with the fact that the real length of the flow path is unknown and the straight-line assumption for the calculation of velocity represents a minimum estimate. Consequently, any modeled transit velocity overestimates the measured data. Model scenarios that account for a possible sinuosity of the flow path yield lower transit velocities, but at the expense of a reduced amplitude of the diurnal variation (Table 3).

[52] Further uncertainty is attributed to the choice of roughness (equation (2)) and flow law parameters (equation (1)) and the assumption of a semicircular channel cross section. Enhanced wall roughness increases the resistance to flow of the channel and, therefore, reduces the transit velocity. However, the hydraulic gradient required to drive the flow increases. Softer ice allows enhanced closure rates, channels become smaller, and from continuity, the transit velocity increases; however, the head has to increase to drive the flow through the smaller channels. The same results are obtained from modeling broad and low channels [*Hooke et al.*, 1990] using an enhanced value for B. Thus, changes in sinuosity, channel roughness and ice stiffness which affect the water pressure in a similar way have opposing effects on transit velocity. *Clarke* [2003] found that the value of the roughness parameter is affected by the choice of the cross-sectional shape of the channel and also by different heat transfer assumptions.

[53] We note that the parameter variations (Table 3) do not reveal a noticeable effect on the v-Q phase relationship and none of the different scenarios generates a v-Q phase shift that is in close proximity to the observation. Furthermore, $S = 3$ is the only scenario that yields transit velocities in a magnitude comparable to the measured values. However, the amplitude of the modeled velocity variation is only approximately 1/3 of the measured variation.

[54] The complex interrelation between different parameters demonstrates that without further constraints on the real flow path and channel geometry, fitting the model to measured data would not provide additional insight. The inability of R channel hydraulics to reproduce the magnitude of observed transit velocities is in line with previous studies which report that calculated velocities consistently overesti-

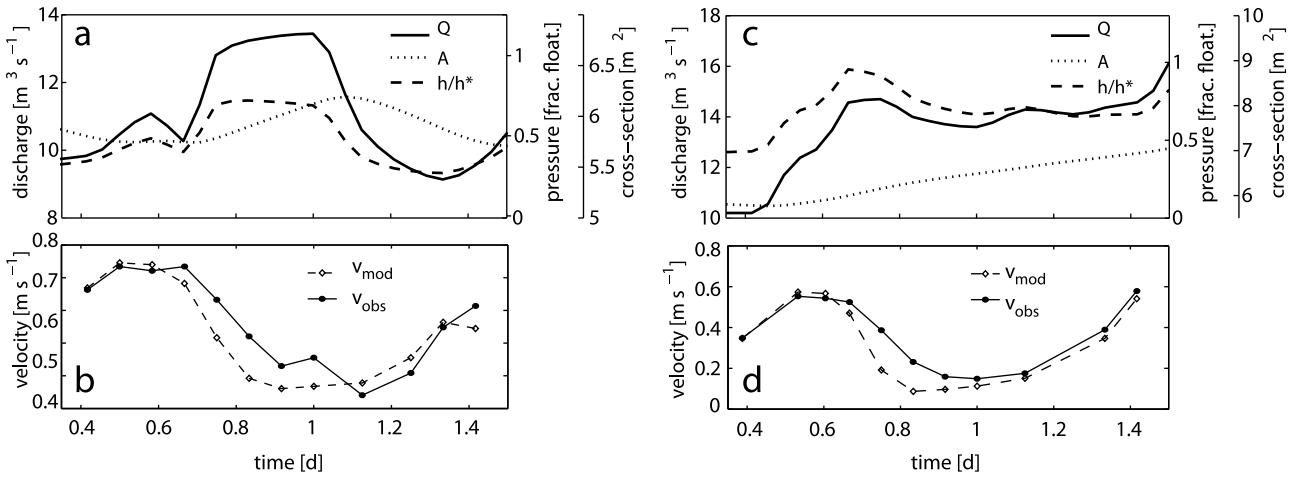

Figure 6. Results of modeling the combined effects of channel geometry changes and inflow modulation for (left) *Exp_1* and (right) *Exp_2*. (a and c) Variations in hydraulic head (expressed as fraction of flotation pressure) h/h^* and cross-sectional area A of a R channel in response to discharge Q. The displayed values of h and A are those calculated for a distance of 4.5 km from the terminus. (b and d) Comparison of modeled (v_{mod}) and observed (v_{obs}) tracer transit velocities.

mate observed values by up to an order of magnitude [*Willis et al.*, 1990; *Fountain*, 1993; *Vatne et al.*, 1995; *Nienow et al.*, 1996].

5.2. Inflow Modulation

[55] Over a wide range of moulin sizes, inflow modulation has a considerable effect on the transit velocity in terms of magnitude and phase with respect to proglacial discharge (Figure 5). If the transit time through the moulin is a large enough fraction of the overall transit time, the influence of the channel on the transit velocity through the entire system is small. The transit time through the moulin depends directly on the water volume in the moulin, $A_M\, h_M$ (equations (8) and (9)). For an infinitely small moulin (e.g., $A_M = 0$ in Figure 5b), $dz_T/dt \rightarrow \infty$ (equation (9)), i.e. the tracer does not experience retardation in the moulin. Hence, v equals the velocity in the channel and varies in phase with Q and h_M. Conversely, for a large moulin (e.g., A_M = 25 m^2 in Figure 5b), the water volume $A_M h_M$ is large for any considerable h_M. Hence, v is reduced (equation (9)) and varies inversely to h_M and Q. For intermediate values of A_M, the influence of Q_{in} on Q_{out} (equation (8)), and hence on the timing of v becomes significant. We recall that the close correlation between v and Q_{in} is one of the key observations stated in Section 2, thereby constraining A_M.

[56] The idea of a moulin being a vertical slot of uniform cross section is certainly an oversimplification. However, if A_M is understood as an effective cross section $A_{M,eff} = A_{M,inc}/\cos\,\Phi$ our formulation applies also to an inclined moulin. Here, the angle Φ denotes the deviation from vertical and $A_{M,inc}$ is the cross-sectional area of the inclined moulin.

5.3. Simulation of *Exp_1* and *Exp_2*

[57] Above, we have investigated the effects of adjustable channel geometry and inflow modulation on transit velocity in separate analyses, before the two mechanisms are combined to simulate *Exp_1* and *Exp_2*. Evaluating the model performance in reproducing the observed range of v as well as the phase relationship between v and Q, we obtain good agreement using S = 1.6 and A_M = 4 m^2 and 5 m^2 for the simulation of *Exp_1* and *Exp_2*, respectively. These choices appear physically plausible with the different values for A_M likely reflecting the enlargement of the moulin over the one month period between the experiments. The sinuosity S = 1.6 indicates that the flow path is considerably longer than the straight line distance between the sites of tracer injection and detection, though its effect on v is only moderate (Table 3). However, the obtained value for S cannot be considered a direct estimate of the real sinuosity since S was treated as the parameter that encompasses all uncertainties related to channel hydraulics.

[58] The results suggest that the residence time of the tracer in the moulin is a considerable fraction of the total residence time. This is the case especially during night, when the moulin input Q_{in} is low, and calculated residence times in the moulin account for more than 50% of the total residence time. This ratio reaches up to ~70% for *Exp_1* and 90% for *Exp_2*. The higher percentage for *Exp_2* is presumably a result of overall higher water pressures due to the rising discharge trend. Higher water pressures are equivalent to a higher water column in the moulin through which the tracer has to travel, thereby increasing the residence time in the moulin.

[59] Considering the simplifying assumptions made in our model, several parameters such as channel roughness, sinuosity or moulin geometry are not well constrained, and hence, there is uncertainty about the exact partitioning of residence times between the moulin and the channel. Unfortunately, additional measurements to further constrain our simulations of *Exp_1* and *Exp_2* are not available. Nevertheless, based on our results, we propose additional measurements that could be made to further enhance the information yield of similar tracer experiments. In principle, the information yield would become larger if the residence time partitioning between the two mechanisms was known. The obvious case is to inject the tracer directly into the channel thereby bypassing the moulin, such that the residence time in the moulin equals zero. This could be achieved for instance by pumping the tracer to the bottom of a borehole that penetrates a subglacial channel,

though the practical implementation of this idea may be difficult. Furthermore, a record of water level fluctuations in the moulin would provide a better constraint on the inflow modulation mechanism, especially if it is accompanied with detailed information of the geometry of the moulin. Since the evolution of inflow modulation is influenced by the variations of h_M and Q_{in}, keeping at least one of these variables constant would increase the certainty about the effects of inflow modulation. So, any situation that satisfies these conditions represents a promising opportunity to conduct series of tracer injections.

6. Conclusions

[60] In this paper, we used numerical modeling to analyze two mechanisms that have been suggested to account for the complexity of diurnal v-Q relationships observed at Unteraargletscher. The modeling work supports the hypothesis that the adjustable geometry of an R channel could be responsible for the hysteresis in the v-Q relationships derived from tracer experiments. However, the hysteresis induced by channel geometry changes is considerably smaller than that derived from measurements. In addition, it appears to be stable over a wide range of accepted values for model parameters such as the roughness coefficient, channel sinuosity, and flow law coefficient (Table 3). Therefore, we conclude that this mechanism may contribute to the observed complexity in the v-Q relation, but it is not the exclusive cause. The difficulty in explaining observed transit velocities by R channel hydraulics (Table 3) strongly suggests that other mechanisms are significant.

[61] Furthermore, the model results show that inflow modulation at the junction of a tributary moulin to the main channel is efficient in affecting transit velocity in magnitude and timing. Typically, supraglacial and proglacial discharge do not vary in phase, and inflow modulation therefore gives rise to complex v-Q relationships. For a suitable choice of A_M, simulated transit velocities are closer to measured values and vary in phase with Q_{in}, in agreement with observations.

[62] When considering both mechanisms, model results indicate that inflow modulation has a dominating effect on the residence time of the tracer, although there is uncertainty about the exact partitioning of residence times in the channel and the moulin. Hence, it is difficult to infer hydraulic conditions of subglacial drainage from experiments conducted in a combined system where inflow modulation plays an important role. To enhance the information yield of similar tracer tests in the future, we recommend additional measurements that enable a better discrimination between the individual components of such a combined drainage system.

[63] **Acknowledgments.** The assistance of T. Khazaleh, J. Helbing, and L. Mutter during our field work is gratefully acknowledged. This study was partly funded by ETH grant TH-6/98-2. The authors are indebted to G.K.C. Clarke for providing the code that was used at an early stage of this study. We also acknowledge stimulating discussions with M. Werder. Further, we are grateful to J. Kohler, P. Nienow, I. Willis, anonymous reviewers, and the Editor for their comments and suggestions that helped to improve the manuscript.

References

Arnold, N. S., K. S. Richards, I. C. Willis, and M. J. Sharp (1998), Initial results from a distributed, physically based model of glacier hydrology, *Hydrol. Processes*, *12*, 191–219.

Bauder, A., M. Funk, and G. Gudmundsson (2003), The ice thickness distribution of Unteraargletscher, Switzerland, *Ann. Glaciol.*, *37*, 331–336.

Boulton, G. S. (1974), Processes and patterns of glacial erosion, in *Glacial Geomorphology*, edited by D. R. Coates, pp. 41–87, State Univ. of New York, Binghampton.

Burkimsher, M. (1983), Investigations of glacier hydrological systems using dye tracer techniques: Observations at Pasterzengletscher, Austria, *J. Glaciol.*, *29*(103), 403–416.

Chow, V. T. (1988), *Open Channel Hydraulics*, McGraw-Hill, Boston.

Chow, V. T., D. R. Maidment, and L. W. Mays (1988), *Applied Hydrology*, McGraw-Hill, Boston.

Clarke, G. K. C. (1987), Subglacial till: A physical framework for its properties and processes, *J. Geophys. Res.*, *92*(B9), 9023–9036.

Clarke, G. K. C. (1996), Lumped-elements analysis of subglacial hydraulic circuits, *J. Geophys. Res.*, *101*(B8), 17,547–17,559.

Clarke, G. K. C. (2003), Hydraulics of subglacial outburst floods: New insights from the Spring-Hutter formulation, *J. Glaciol.*, *49*(165), 299–313.

Collins, D. N. (1982), Flow-routing of meltwater in an alpine glacier as indicated by dye tracer tests, *Beitr. Geol. Schweiz-Hydrol.*, *28*(2), 523–534.

Cutler, P. (1998), Modelling the evolution of subglacial tunnels due to varying water input, *J. Glaciol.*, *44*(148), 485–497.

Fountain, A. G. (1993), Geometry and flow conditions of subglacial water at South Cascade Glacier, Washington State, U.S.A: An analysis of tracer injections, *J. Glaciol.*, *39*(131), 143–156.

Gudmundsson, G. H. (1999), A three-dimensional numerical model of the confluence area of Unteraargletscher, Bernese Alps, Switzerland, *J. Glaciol.*, *45*(150), 219–230.

Hock, R., and R. L. Hooke (1993), Evolution of the internal drainage system in the lower part of the ablation area of Storglaciären, Sweden, *Geol. Soc. Am. Bull.*, *105*(4), 537–546.

Hock, R., A. Iken, and A. Wangler (1999), Tracer experiments and borehole observations in the overdeepening of Aletschgletscher, Switzerland, *Ann. Glaciol.*, *28*, 253–260.

Hooke, R. L., T. Laumann, and J. Kohler (1990), Subglacial water pressures and the shape of subglacial conduits, *J. Glaciol.*, *36*(122), 67–71.

Iken, A., and R. A. Bindschadler (1986), Combined measurements of subglacial water pressure and surface velocity of Findelengletscher, Switzerland: Conclusions about drainage system and sliding mechanism, *J. Glaciol.*, *32*(110), 101–119.

Iken, A., H. Röthlisberger, A. Flotron, and W. Haeberli (1983), The uplift of the Unteraargletscher at the beginning of the melt season: A consequence of water storage at the bed?, *J. Glaciol.*, *29*(101), 28–47.

Iverson, N. R., B. Hanson, R. L. Hooke, and P. Jansson (1995), Flow mechanism of glaciers on soft beds, *Science*, *267*(5194), 80–81.

Joughin, I., S. B. Das, M. A. King, B. E. Smith, I. M. Howat, and T. Moon (2008), Seasonal speedup along the western flank of the Greenland ice sheet, *Science*, *320*(5877), 781–783, doi:10.1126/science.1153,288.

Kavanaugh, J. L., and G. K. C. Clarke (2001), Abrupt glacier motion and reorganisation of basal shear stress following the establishment of a connected drainage system, *J. Glaciol.*, *47*(158), 472–480.

Kohler, J. (1995), Determining the extent of pressurized flow beneath Storglaciären, Sweden, using results of tracer experiments and measurements of input and output discharge, *J. Glaciol.*, *41*(138), 217–231.

Lang, H., C. Leibundgut, and E. Festel (1979), Results from tracer experiments on the water flow through the Aletschgletscher, *Z. Gletscherkd. Glazialgeol.*, *16*(2), 209–218.

Mair, D., P. Nienow, M. Sharp, T. Wohlleben, and I. Willis (2002), Influence of subglacial drainage system evolution on glacier surface motion: Haut Glacier d'Arolla, Switzerland, *J. Geophys. Res.*, *107*(B8), 2175, doi:10.1029/2001JB000514.

Ng, F. (2000), Canals under sediment-based ice-sheets, *Ann. Glaciol.*, *30*, 146–152.

Nienow, P. W., M. Sharp, and I. C. Willis (1996), Velocity-discharge relationships derived from dye tracer experiments in glacial meltwaters: Implications for subglacial flow conditions, *Hydrol. Processes*, *10*, 1411–1426.

Nienow, P. W., M. Sharp, and I. C. Willis (1998), Seasonal changes in the morphology of the subglacial drainage system: Haut Glacier d'Arolla, Switzerland, *Earth Surf. Processes Landforms*, *23*, 825–843.

Nye, J. F. (1953), The flow law of ice from measurements in glacier tunnels, laboratory experiments and the Jungfraufirn borehole experiment, *Proc. R. Soc. London, Ser. A*, *219*(1193), 477–489.

Nye, J. F. (1973), Water at the bed of a glacier, in *Symposium on the Hydrology of Glaciers, Cambridge 1969*, *IASH Publ.*, *95*, 189–194.

Nye, J. F. (1976), Water flow in glaciers: Jökulhlaups, tunnels and veins, *J. Glaciol.*, *17*(76), 181–207.

Paterson, W. S. B. (1994), *The Physics of Glaciers*, 3rd ed., 480 pp., Pergamon, New York.

Röthlisberger, H. (1972), Water pressure in intra– and subglacial channels, *J. Glaciol.*, *11*(62), 177–203.

Schiesser, W. (1991), *The Numerical Method of Lines*, Academic, San Diego, Calif.

Schuler, T., and U. H. Fischer (2002), Elucidating changes in the degree of tracer dispersion in a subglacial channel, *Ann. Glaciol.*, *37*, 275–280.

Schuler, T., U. H. Fischer, and G. H. Gudmundsson (2004), Diurnal variability of subglacial drainage conditions as revealed by tracer experiments, *J. Geophys. Res.*, *109*, F02008, doi:10.1029/2003JF000082.

Seaberg, S. Z., J. Z. Seaberg, R. L. Hooke, and D. W. Wiberg (1988), Character of the englacial and subglacial drainage system in the lower part of the ablation area of Storglaciären, Sweden, as revealed by dye-trace studies, *J. Glaciol.*, *34*(117), 217–227.

Smart, C. (1990), Comments on: "Character of the englacial and subglacial drainage system in the lower part of the ablation area of Storglaciären, Sweden, as revealed by dye-trace studies", *J. Glaciol.*, *36*(122), 126–128.

Spring, U. (1980), Intraglazialer Wasserabfluss: Theorie und Modellrechnung, *Mitteilung 48*, Versuchsanstalt für Wasserbau, Hydrologie und Glaziologie der ETH Zürich, Zürich, Switzerland.

Spring, U., and K. Hutter (1982), Conduit flow of a fluid through its solid phase and its application to intraglacial channel flow, *Int. J. Eng. Sci.*, *20*, 327–363.

Tranter, M., G. H. Brown, R. Raiswell, M. J. Sharp, and A. M. Gurnell (1993), A conceptual model of solute acquisition by alpine glacial meltwaters, *J. Glaciol.*, *39*(133), 573–581.

Truffer, M., W. D. Harrison, and R. March (2005), Record negative glacier balances and low velocities during the 2004 heatwave in Alaska, USA: Implications for the interpretation of observations by Zwally and others in Greenland, *J. Glaciol.*, *51*(175), 663–664.

van de Wal, R. S. W., W. Boot, M. van den Broeke, C. Smeets, C. Reijmer, J. Donker, and J. Oerlemans (2008), Large and rapid melt-induced velocity changes in the ablation zone of the Greenland ice sheet, *Science*, *321*, 111–113.

Vatne, G., B. Etzelmüller, J. Sollid, and R. Ødegård (1995), Hydrology of a polythermal glacier, Erikbreen, northern Spitsbergen, *Nordic Hydrol.*, *26*, 169–190.

Walder, J. S. (1986), Hydraulics of subglacial cavities, *J. Glaciol.*, *32*(112), 439–445.

Walder, J. S., and A. Fowler (1994), Channelized subglacial drainage over a deformable bed, *J. Glaciol.*, *40*(134), 3–15.

Weertman, J. (1972), General theory of water flow at the base of a glacier or ice sheet, *Rev.Geophys.*, *10*(1), 287–333.

Willis, I. C., M. J. Sharp, and K. S. Richards (1990), Configuration of the drainage system of Midtalsbreen, Norway, as indicated by dye-tracing experiments, *J. Glaciol.*, *36*(122), 89–101.

Zwally, H. J., W. Abdalati, T. Herring, K. Larson, J. Saba, and K. Steffen (2002), Surface melt-induced acceleration of Greenland ice sheet flow, *Science*, *297*(5579), 218–222.

U. H. Fischer, National Cooperative for the Disposal of Radioactive Waste, Hardstrasse 73, CH-5430 Wettingen, Switzerland. (urs.fischer@nagra.ch)

T. V. Schuler, Department of Geosciences, University of Oslo, P.O. Box 1047 Blindern, N-0316 Oslo, Norway. (t.v.schuler@geo.uio.no)